Lab on a Chip

Integration of 3D Printed Mg^{2+} Potentiometric Sensors into Microfluidic Devices for Bioanalysis

Journal:	*Lab on a Chip*
Manuscript ID	LC-ART-05-2024-000407.R1
Article Type:	Paper
Date Submitted by the Author:	09-Jul-2024
Complete List of Authors:	Farahani, Sarah; Washington State University, Chemistry Glasco, Dalton; Washington State University, Chemistry Elhassan, Manar; The British University in Egypt, Analytical Chemistry Sireesha, Pedaballi; Washington State University, Chemistry Bell, Jeffrey; Washington State University, Chemistry

ARTICLE

Integration of 3D Printed Mg^{2+} Potentiometric Sensors into Microfluidic Devices for Bioanalysis

Received 00th January 20xx,
Accepted 00th January 20xx

DOI: 10.1039/x0xx00000x

Sarah Farahani[1], Dalton L. Glasco[1], Manar M. Elhassan[1,3], Pedaballi Sireesha[1], Jeffrey G. Bell[1,2,*]

[1] Department of Chemistry, Washington State University, Pullman, Washington, 99164, United States.
[2] The Gene and Linda Voiland School of Chemical Engineering and Bioengineering, Washington State University, Washington 99164, United States
[3] Pharmaceutical Analytical Chemistry Department, Faculty of Pharmacy, The British University in Egypt, El-Sherouk City, 11837, Egypt

[*] Corresponding Author: jeffrey.g.bell@wsu.edu

Electrochemical sensors provide an affordable and reliable approach towards the detection and monitoring of important biological species ranging from simple ions to complex biomolecules. The ability to miniaturize electrochemical sensors, coupled with their affordability and simple equipment requirements for signal readout, permits the use of these sensors at the point-of-care where analysis using non-invasively obtainable biofluids is receiving growing interest by the research community. This paper describes the design, fabrication, and integration of a 3D printed Mg^{2+} potentiometric sensor into a 3D printed microfluidic device for the quantification of Mg^{2+} in low-sample volume biological fluids. The sensor employs a functionalized 3D printable photocurable methacrylate-based ion-selective membrane affixed to a carbon-mesh/epoxy solid-contact transducer for the selective determination of Mg^{2+} in sweat, saliva and urine. The 3D printed Mg^{2+} ion-selective electrode (3Dp-Mg^{2+}-ISE) provided a Nernstian response of 27.5 mV/decade with a linear range of 10 mM to 39 µM, covering the normal physiological and clinically relevant levels of Mg^{2+} in biofluids. 3Dp-Mg^{2+}-ISEs selectively measure Mg^{2+} over other biologically present cations – sodium, potassium, calcium, ammonium – as well as provided high stability in the analytical signal with a drift of just 13 µV/h over 10 hours. Comparison with poly(vinylchloride)-based Mg^{2+}-ISEs showed distinct advantages to the use of 3Dp-Mg^{2+}-ISEs, with respect to stability, resilience towards biofouling and importantly provides a streamlined and rapid approach towards mass production of selective and reliable sensors. The miniaturization capabilities of 3D printing coupled with the benefits of microfluidic analysis (i.e., low sample volumes, minimal reagent consumption, automation of multiple assays, etc.), provides exciting opportunities for the realization of the next-generation of point-of-care diagnostic devices.

1. Introduction

Magnesium (Mg^{2+}) is the fourth most prevalent cation in the body and the second most abundant intracellular cation and is physiologically necessary for numerous bodily processes including its function as a cofactor for over 300 enzyme reactions [1]. Mg^{2+} is necessary for the production of proteins and nucleic acids, for intermediate metabolism, and for specific processes in various organ systems, including the cardiovascular and neuromuscular systems [2]. Despite its significance, it still has not received the attention it deserves in clinical practice or the medical literature, and routine laboratory testing often does not involve the determination of serum Mg^{2+} concentration [3]. Hypomagnesemia, which is a low Mg^{2+} level in the blood (0.75 mmol/L) [4] is characterized by many symptoms such as tremors, depression, encephalopathy, seizures, cardiac arrhythmia, and ECG changes [2]. Moreover, Mg^{2+} imbalances have been reported to be associated with higher mortality and longer hospital stays in patients admitted to the intensive care unit [5], [6].

[a] *Address here.*
[b] *Address here.*
[c] *Address here.*
† Footnotes relating to the title and/or authors should appear here.
Electronic Supplementary Information (ESI) available: [details of any supplementary information available should be included here]. See DOI: 10.1039/x0xx00000x

Despite its prevalence, hypomagnesemia commonly does not receive intensive research attention due to the absence of symptoms until serum levels are significantly low (< 0.62 mmol/L) [7] or a general poor comprehension of Mg^{2+} physiology or both [8].

Unfortunately, there are many challenges in the determination of Mg^{2+} level in the body, which are derived from the fact that about 40–50% of the total Mg^{2+} content is stored in muscles and other soft tissues, and the remaining 50–60% is stored in bones. The extracellular Mg^{2+} in the body is made up of less than 2% of Mg^{2+} and is found primarily in serum (~0.3%) and red blood cells. Therefore, because only 0.3% of the body's total Mg^{2+} is found in serum, patients can have normal serum Mg^{2+} levels, but the cells are depleted of Mg^{2+}[2]. To address those challenges, an important test, called the 24-hour urine magnesium output measurement or magnesium tolerance test, is carried out. This test involves the parenteral magnesium loading dose intake followed by urine collection for the next 24 hours. It was found that compared to normal participants, hypomagnesemic subjects retained noticeably more of the magnesium that was given to them. Therefore, urine was proposed as an important biofluid for the determination of Mg^{2+} [9],[10].

To address challenges in detecting physiological Mg^{2+} levels, researchers have investigated various separation-based analytical approaches such as high-performance liquid chromatography (HPLC) [11], [12], as well as various sensors, including electrochemical sensors [13], [14], [15], optical sensors [16], colorimetric [17], and fluorescent chemosensors [18], [19]. Of these approaches, electrochemistry plays a pivotal role in analytical chemistry, offering many advantages such as high reproducibility and selectivity [20], [21]. Electrochemical methods are characterized by their exceptional sensitivity, enabling the detection of trace amounts of analytes, even in complex matrices. Furthermore, electrochemical techniques often exhibit excellent selectivity [22], allowing for the specific identification and quantification of target substances amidst a variety of interferences. The versatility of electrochemical sensors and electrodes [23] facilitates the detection of a wide range of analytes, from ions to organic molecules, contributing to the method's broad applicability. Additionally, electrochemical analyses are often cost-effective [24], as they can be performed with relatively simple instrumentation compared to alternative methods such as HPLC which require expensive equipment and trained personnel to operate.

Potentiometry, a powerful electrochemical technique for the detection of ionic species, uses ion-selective electrodes (ISEs) that have seen diverse implementation in electroanalysis. ISEs provide many advantages, including fast and reliable analysis, high selectivity and sensitivity, and seamless transition to point-of-care (POC) devices for on-site diagnostics [25], [26]. Many researchers have developed Mg^{2+}-ISEs due to magnesium's importance in numerous physiological disorders and diseases. Conventionally, polyvinyl chloride (PVC) is used as the structural support material in the fabrication of the ISEs sensing element (ion-selective-membrane, ISM). However, the reliance on PVC in the construction of ISMs results in inherent difficulties in the realization of mass production capabilities [25]. Over the past 5 years, 3D printing has emerged as a transformative technology in the field of electrochemistry, revolutionizing the design and fabrication of devices critical to energy storage, conversion, and sensing applications. The versatility of 3D printing allows for the precise and customizable production of intricate electrode structures, improving electrochemical systems' overall efficiency and performance [27]. This technology enables the fabrication of complex geometries and architectures, optimizing the surface area, porosity, and conductivity of electrodes. The ability to rapidly prototype and iterate designs enhances the exploration of novel materials and configurations, accelerating advancements in electrochemical research [27]. As a result, 3D printing has become an indispensable tool in the field of electrochemistry, offering unprecedented opportunities for tailoring electrochemical devices to meet specific application requirements [25]. Recently, the ability of endowing 3D printable materials with the functional components of ISMs (e.g., ion-exchanging salts, plasticizers, and ionophores), has resulted in the realization of 3D-printed ISEs (3Dp-ISEs). To date, 3Dp-ISEs have only been developed for Ca^{2+} [28], K^{+}, bilirubin [25], benzalkonium [29], apomorphine [30] and acetylcholine [31]. These ISEs have demonstrated great stability, selectivity and suitable detection ranges for the specific applications and have been used in various biological fluids such as plasma and whole blood although their robustness towards resisting biofouling has yet to be investigated. Moreover, there are no reports on the integration of 3Dp-ISEs into microfluidic devices, where low sample volumes and maintained analytical performance [32] provide clinical setup miniaturization and automate multiple assays. Microfluidics is a scientific field that focuses on the investigation and manipulation of fluid dynamics and particles at minuscule length scales ranging from tens to hundreds of micrometers paving the way to noninvasive and sensitive analysis for different bioanalytical applications. [33]. Due to their advantages, including high throughput, portability, quick sample processing and analysis, low fabrication costs, reduced sample volume, and enhanced integration and functionality of multiple devices and components into a single chip, microfluidic chips are being used in biochemical processes and miniaturized analytical methods [34]. These advantages permit interrogation of biofouling with minimally abundant (and non-invasively obtainable) biofluids such as saliva and sweat. The increasing use of non-invasive biofluids in (bio)analysis has numerous advantages including being painless, a decreased risk of infection, and easily obtainable by patient (i.e., no need for trained personnel to withdraw sample).

This paper reports the first 3D printed Mg^{2+}-ISE (3Dp-Mg^{2+}-ISE), fabricated using stereolithography-based 3D printing, which was evaluated in various biological fluids (e.g., saliva, sweat, urine and blood plasma). The fabricated 3Dp-Mg^{2+}-ISE exhibited a Nernstian response over the physiologically relevant concentrations of Mg^{2+} present in the investigated biofluids. The performance of the 3Dp-Mg^{2+}-ISE was compared to a PVC-Mg^{2+}-ISE to determine differences in resilience towards biofouling and long-term stability. The integration of the 3Dp-Mg^{2+}-ISE into a 3D printed microfluidic device represents an important step towards the realization of fully 3D printed analytical devices.

2. Experimental

2.1. Materials and Reagents

Magnesium chloride (MgCl2) was purchased from VWR international, USA. Magnesium ionophore I (C49H94N6O6), bis-2-ethylhexyl sebacate (DOS, C26H50O4, >97.0%), potassium tetrakis (4-chlorophenyl) borate (KTClPB, C24H16BCl4K, > 98.0%), Poly(vinylchloride), PVC, tetrahydrofuran (THF), and potassium chloride (KCl) were all purchased from Sigma Aldrich. A photocurable resin (Flexible 80A) base of an acrylate monomer (79-95%), urethane dimethacrylate (3-6%), and photoinitiator (<1.5) and a photopolymer resin clear (FLGPCL04) based of Methacrylate Oligomer(s) (10-15%), Methacrylate Monomer(s) (65-85%), Urethane dimethacrylate (10-15 %), and Ethyl phenyl(2,4,6-trimethylbenzoyl)phosphinate (<3) were purchased from Formlabs. Sodium chloride (NaCl) and calcium chloride (CaCl2) were purchased from EMD Millipore, Germany. Ammonium chloride (NH4Cl) was purchased from MACRON Fine Chemicals, and acetylcholine bromide (C7H16BrNO2) was purchased from TCI. All solutions were prepared using distilled (DI) water. Isopropyl Alcohol (IPA) was purchased from Fisher Chemical. Carbon mesh (PAN Graphite Felt – 3.1 mm thick) was purchased from Fuel Cell, United States. Single-donor human Saliva and pooled Human Urine were purchased from Innovative Research Lab, Incorporation. Normal Sweat was purchased from Medix Biochemica.

2.2. Equipment and Instrumentation

A 16-channel potentiometer was purchased from Lawson Labs and a single-channel of this device is used to measure the electromotive force (*emf*) vs time data for each of the fabricated ISEs. A solid-contact Ag/AgCl was purchased from eDAQ Inc. A Form 3 SLA 3D printer was purchased from FormLabs Inc. and was used to print the microfluidic device and the solid-contact housing for the 3Dp-Mg^{2+}-ISEs. A Mars 2 SLA 3D printer purchased from Elegoo Inc. was used to print the Mg^{2+} ion-selective-membrane. A UV oven (Melody Susie) with a wavelength of 365 nm was used to post-cure all 3D printed components after printing.

2.3. Procedures

2.3.1. *Preparation of 3D printable Mg^{2+}-ISM cocktail*

The 3D-printed Mg^{2+}-ISM (3Dp-Mg^{2+}-ISM) was prepared by combining 89.95% photocurable resin (Flexible 80A), 8% DOS, 0.75% KTClPB and 1.3% magnesium ionophore I. To obtain a fully homogenous cocktail, those components were mixed and left to dissolve overnight with constant stirring.

2.3.2. Preparation of PVC-Mg^{2+}-ISM Cocktail

A previously reported procedure for a PVC-Mg^{2+}-ISM composition was followed [35] A mixture of 64.5% wt. NPOE, 33.1% wt. PVC, 1% wt. KTClPB, and 1.4 % magnesium ionophore I was incorporated and dissolved in 5 mL of THF.

2.3.3. 3D Printing and Mg^{2+}-ISE Fabrication

In this work, Fusion360 was utilized to create a computer-aided design (CAD) for different components of a 3D-printed solid-contact Mg^{2+} ISE integrated into a microfluidic device, including i) Mg^{2+} ISM, ii) solid-contact housing, and iii) microfluidic device. Then, using a Mars 2 SLA 3D printer, Mg^{2+} ISM with 0.3 mm of thickness was pre-cured for 30 seconds, followed by washing with IPA. Both solid-contact housing and microfluidic devices were fabricated using a Form 3 SLA 3D printer, which were printed using photopolymer resin clear. The 3D-printed parts were immersed in IPA for 30 minutes and then cured in the UV oven for an additional 30 minutes.

2.3.3.1. 3D printed Mg^{2+} solid contact-ISE fabrication

A carbon mesh paste was created my mixing the fibrous carbon with an epoxy (Eclectic Products) at a 1:2 wt%, following a previously reported protocol [30]. However, the dimensions were optimized to integrate the sensor into a microfluidic device. The sensors were conditioned overnight in 100 µM $MgCl_2$.

2.3.3.2. PVC Mg^{2+} solid contact-ISE fabrication

To fabricate a PVC membrane with roughly 0.3 mm thickness, 100 µL of the Mg^{2+} ISM cocktail was drop cast onto the 3D-printed SC-ISE housing and set for 30 minutes. Afterward, the PVC-Mg^{2+}-ISEs were conditioned overnight in a 100 µM $MgCl_2$.

2.3.3.3. Microfluidic Device Fabrication

The microfluidic device was optimized to incorporate the entire potentiometric setup (reference electrode and ISE) while minimizing sample volume. The rectangular-based microchannel (40 mm, 5.0 mm, 1 mm) has a volume of 220 mm^3 and is a pipette-based operated device, which simplifies operation. The liquid injection process was conducted with a syringe with a 1 mm (25 gauge) needle attached. Figure SI.1 shows a detailed schematic of the microfluidic device, including dimensions.

2.3.4. Selectivity Studies

The selectively of the Mg^{2+}-ISEs was evaluated by conditioning them in a solution of 1 mM KCl overnight and then measuring the *emf* values for 1 mM potassium, sodium, ammonium, calcium, acetylcholine and magnesium. To ensure no cross-contamination, the beaker was rinsed with DI water and dried between measurements of different cations. To determine the selectivity coefficients for each possible interferent, we used the following formula (Equation (1)):

$$logK_{a,x}^{pot} = \frac{Z_a(E_x - E_a)}{59.2} + \log\left(\frac{C_a}{C_x^{\left(\frac{Z_a}{Z_x}\right)}}\right) \quad \text{Equation (1)}$$

In this formula, K^{pot} is the selectivity coefficient, Z_a is the charge of the analyte, Z_x is the charge of the interfering ion, E_a is the *emf* response to the analyte, E_x is the *emf* response to the interfering ion, C_a is the concentration of the analyte, and C_x is the concentration of the interfering ion.

2.3.5. Water Layer Test and Stability

To determine the presence or absence of a water layer, a conditioned Mg^{2+}-ISEs were immersed in 1 mM $MgCl_2$ for a duration of 3 hours and the resulting *emf* response was measured. The sensor was subsequently submerged in a solution of 1 mM KCl for 3 hours and then back in 1 mM $MgCl_2$ for another 3 hours. The continuous monitoring of the *emf*, where no drift was observed, indicates no water layer in the sensor. To evaluate stability, the *emf* response of Mg^{2+}-ISEs in a 1 mM solution of $MgCl_2$ was recorded over a 10-hour period.

2.3.6. Calibration of PVC-Mg^{2+}-ISEs

For the calibration of Mg^{2+}, solid-contact Ag/AgCl was utilized as the reference electrode. The calibration started with 10 mLs of a 10 mM Mg^{2+} solution, then performed 1:1 dilution by withdrawing 5 mL of the existing solution and adding 5 mL DI water followed by stirring the solution. The *emf* response following each dilution was recorded.

2.3.7. Calibration of 3Dp-Mg^{2+}-ISEs in a 3D printed microfluidic device

The functionality of the sensor inside the microfluidic device was evaluated by obtaining a calibration curve starting with 10 mM $MgCl_2$ using a solid-contact Ag/AgCl as the reference electrode. For optimal results, the calibration process was executed at a 1:1 dilution using the same solid-contact Ag/AgCl reference electrode until the process was completed. In this process, the solution is flowed through the microfluidic channel to fill the whole channel, and the *emf* response was recoded under no-flow conditions. To ensure the accuracy of the experiment, the channel was washed with DI water and dried after every step of liquid injection to prevent any changes in the actual concentration.

2.3.8. Biofouling Analysis

Calibration curves taken before and after soaking the Mg^{2+}-ISEs in individual biological fluids for 12 hours were obtained. Calibration curves were obtained following the protocols previously stated. Stability experiments were also performed in sweat, saliva and urine solutions containing 1 mM Mg^{2+}.

3. Results and Discussion

3.1 Sensing mechanism and response of 3Dp-Mg^{2+}-ISEs

Potentiometric sensors are valuable tools for the selective detection and monitoring of ionic species, such as Mg^{2+}. To fabricate our Mg^{2+} selective electrode we developed and optimized a 3D printable Mg^{2+}-ISM cocktail (Figure 1Ai) containing four functional components, i) photocurable methacrylate-based resin, ii) an ion-exchanging salt, iii) a plasticizer, and iv) a Mg^{2+} ionophore. The photocurable methacrylate-based resin serves as the structural support of the ISM, the plasticizer (bis(ethylhexyl) sebacate, DOS) helps to dissolve the ISM components and provide improved mobility, the hydrophobic ion-exchanging anion (tetrakis(4-chlorophenyl)borate, TClPB) establishes cationic permselectivity and establishes a constant concentration of Mg^{2+} in the ISM, and the Mg^{2+} ionophore provides enhanced selectivity towards Mg^{2+} ions over other cationic species. Once the Mg^{2+} cocktail was homogenous it was incorporated into the 3D printer and based off a pre-designed CAD file, disk shaped Mg^{2+}-ISMs were printed. There are two main differences between the compositions of 3D printed ISMs and PVC-based ISMs, namely the amount of plasticizer. 89.95% of the 3D printable ISM cocktail is composed of the photocurable methacrylate resin with 8% plasticizer (the remainder is the KTClPB and ionophore). The PVC-based ISM contains a much higher amount of plasticizer (~65%) and ~33% of the PVC polymer. To construct the solid-contact Mg^{2+}-ISEs (both 3D printed and PVC-based), their respective Mg^{2+}-ISMs were affixed to a 3D printed housing which contains a carbon mesh and epoxy mixture, serving as the ion-to-electron transducer (Figure 1Bi). We previously reported on the use of the 3D printed housing and ion-to-electron transducer, however the dimensions were miniaturized for incorporation into the microfluidic device schematically represented in Figure 1Bii. Figure 1C shows a schematic representation of the experimental setup including both reference and 3Dp-Mg^{2+}-ISEs. Figure SI.2 shows an image of the experimental setup.

To achieve the optimal response towards Mg^{2+}, we adjusted various parameters and assessed the effectiveness of the Mg^{2+}-ISEs based on linear range, limit of detection (LOD), and the slope of the resulting calibration curve. The ideal slope should be 29.6

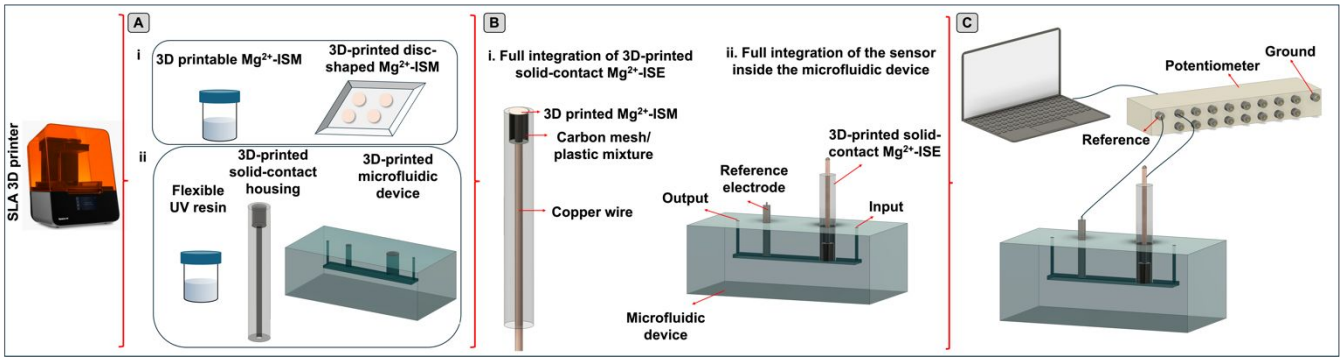

Figure 1. Schematic representation of 3Dp-Mg $^{2+}$- ISE integrated into the microfluidic device. Ai. Represents the 3D printing process for ISM fabrication using an SLA 3D printer. Aii. Represents 3D printing process for the fabrication of electrode housing and microfluidic device using an SLA 3D printer. Bi. Integration of 3Dp-Mg^{2+}-ISM and its transition into solid-contact ISE. Bii. Integration of 3Dp-Mg^{2+}-ISE into the microfluidic device. C. Experimental setup.

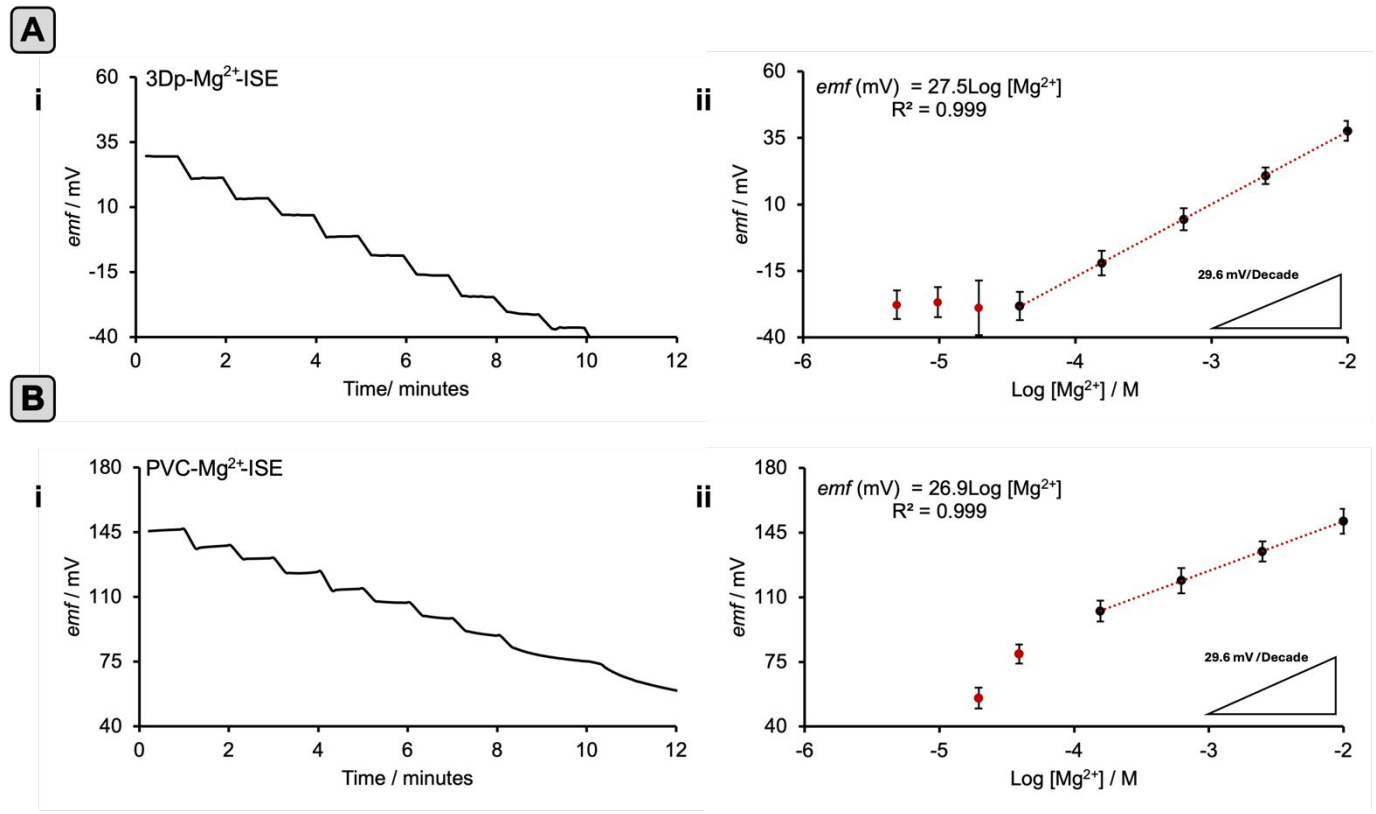

Figure 2. Ai. Time series illustrating the *emf* response of 3Dp-Mg^{2+}-ISE to 1:1 dilutions of a 10 mM Mg^{2+} solution. Aii. The linear response of Mg^{2+} of 3Dp-Mg^{2+}-ISE is linear within the concentration range of 10 mM– 39 µM, showing a slope of 27.5 mV/decade. Bi. Time series data illustrating the *emf* response of PVC-Mg^{2+}-ISE to 1:1 dilutions of a 10 mM Mg^{2+} solution. Bii. The response of Mg^{2+} of PVC-Mg^{2+}-ISE is linear within the 10 mM– 156 µM concentration range, showing a slope of 26.9 mV/decade. Error bars represent the standard deviation across three separate Mg^{2+}-ISEs.

mV/decade, as predicted by the Nernst equation (Equation (2)) for a double-charged analyte, which takes into account the standard potential (E^0, mV), ion's charge (z), and ion's concentration (c).

$$emf = E^0 + \frac{59.2\ mV}{z} \log c \qquad \text{Equation (2)}$$

As previously mentioned, besides substituting methacrylate-based resin for PVC, the primary difference in composition between 3D printable ISMs and PVC-based ISMs is the amount of plasticizer. Interestingly, previous research has demonstrated the detection of analytes (e.g., Na^+, K^+, etc.) using photocurable polymers without the incorporation of plasticizer, referred to as "self-plasticizing". While omitting the incorporation of plasticizer into the ISM cocktail would have a beneficial impact on the overall cost of the resulting ISEs, previous work has demonstrated that 3D printed membranes without plasticizer suffer from less than desirable reproducibility, even after 3D printing [25]. To ensure optimal response and reproducibility, various plasticizer percentages were evaluated. Table SI.1 shows that although 3Dp-Mg^{2+}-ISEs containing 4% and 12% DOS resulting in Nernstian responses, the linearity and linear range were significantly improved with ISMs containing 8%.

Figure 2Ai shows a trace of the *emf* vs. time data for the calibration of the integrated 3Dp-Mg^{2+}-ISE in the microfluidic device. The ISE exhibited a short response time and the *emf* decreased immediately (rapidly becoming stable) after performing a dilution to decrease the concentration of Mg^{2+} in the microfluidic channel. Figure 2Aii displays the linear response of the 3Dp-Mg^{2+}-ISE between 10 mM and 39 µM Mg^{2+} (Illustrated error bars are the standard deviation obtained from three separate Mg^{2+}-ISEs). The slope of *emf* vs. logarithm of Mg^{2+} concentration (M) was 27.5 mV/decade, which is close to the theoretically expected slope of 29.6 mV/decade (inset triangle depicts a slope of 29.6 mV/decade), and thus the 3Dp-Mg^{2+}-ISE behaves in a Nernstian fashion. The linear range covered by the 3Dp-Mg^{2+}-ISE covers the clinically relevant ranges of Mg^{2+} in various biological fluids (Table 1). Figure 2Bi and Figure 2Bii shows the *emf* vs. time data and the linear response

Table1. The clinically relevant ranges of Mg^{2+} in various biological fluids.

	[Mg^{2+}] / mM	[Ca^{2+}] / mM	[K^+] / mM	[Na^+] / mM	[NH_4^+] / mM	[Ach^+] / mM
Saliva	0.05 – 0.19 [36]	0.08 – 2.52 [36]	13 – 16 [37]	8.7 – 24 [37]	--	--
Sweat	0.1 – 0.4 [38]	0.41 – 1.24 [39]	2.63 – 3.87 [40]	9.1 – 39.1[40]	0.5 – 8 [41]	--
Urine	4 [42]	4 [42]	28.82 – 95.22 [43]	7.7 – 129.7 [43]	19 [42]	0.0034 – 0.0039 [44]

obtained for a PVC-Mg^{2+}-ISE.

Table2. Analytical Characteristics for previously reported PVC-Mg^{2+}-ISEs .3

ISE Matrix	Response range / mM	Slope / mV/decade	Detection limit / mM	Reference
PVC	0.01-100	31	--	[45]
PVC	0.0084-100	29.2	--	[46]
PVC	0.032-100	30	0.0063	[47]
PVC	2-20	29.9	1.7	[48]
PVC	0.1-10	28.1	--	[49]
PVC	0.01-100	29.2	0.01	[50]
PVC	0.071-100	27.9	0.0398	[51]
3D Printed	0.039-10	27.5	0.039	Current Work

Although the PVC-Mg^{2+}-ISE had a similar slop (26.9 mV/decade), the linear range was slightly decreased to between 10 mM and 156 μM, which is consistent with other PVC-Mg^{2+}-ISEs reported. A comparison table between previously reported PVC-Mg^{2+}-ISEs and the proposed 3Dp-Mg^{2+}-ISE is shown in Table 2. As can be seen in Table 1, the physiological composition of saliva, sweat and urine contain various cationic species such as calcium, potassium, sodium, ammonium and acetylcholine (more pronounced in urine) at potentially significantly higher concentrations, and ranges, than magnesium. These additional components represent potential interfering species towards the reliable detection, and/or monitoring, of Mg^{2+} in these biological fluids.

3.2 Selectivity of the 3Dp-Mg^{2+}-ISE

To function as a viable sensor, the 3Dp-Mg^{2+}-ISE must have sufficient selectivity over other commonly present potential interferants. Owing to the cationic permselectivity afforded through the use of the KTClB ion-exchanging salt, we investigated common positively charged ions (e.g., K^+, Na^+, NH_4^+ and Ca^{2+}) as well as the positively charged neurotransmitter Ach^+. Figure 3A represents the observed *emf* response of the 3Dp-Mg^{2+}-ISE in 1 mM solutions of KCl, NaCl, NH_4Cl, $CaCl_2$ and Ach^+ bromide versus the *emf* response for a 1 mM $MgCl_2$ solution. Figure 3B shows the *emf* response of the PVC-Mg^{2+}-ISE towards the same cationic interferants as well as Mg^{2+}. Experimentally determined selectivity coefficients were calculated using Equation 1 and are shown in Table 3. Interestingly, the selectivity coefficient obtained against K^+ were similar for both 3D printed and PVC-Mg^{2+}-ISEs, however, there are noticeable differences in the selectivity coefficients for the other interferants. Although the 3Dp-Mg^{2+}-ISE was capable of displaying selectivity towards Mg^{2+} over all other ions, PVC-Mg^{2+}-ISEs demonstrated superior selectivity towards both Na^+ and NH_4^+. Moreover, the PVC-Mg^{2+}-ISE had no selectivity towards Mg^{2+} over Ca^{2+} and Ach^+, whereas the 3Dp-Mg^{2+}-ISE had logK values of -1.98 and -1.65, respectively.

3.3 Stability and Water Layer

Assessing a sensor's stability is of paramount importance, especially in applications where continuous monitoring is required. Figure 4A shows the *emf* response of both the PVC-Mg^{2+}-ISE (red trace) and 3Dp-Mg^{2+}-ISE (black trace) in 1 mM Mg^{2+} monitored over

mV/h)

in the signal obtained with the PVC-Mg^{2+}-ISE. In contrast, the 3Dp-Mg^{2+}-ISE exhibited much greater stability with a total *emf* drift of just 0.13 mV over the course of the measurement, corresponding to a drift of just 13 μV/h. To gain insight into these observations we performed the well-known "water-layer" test. In solid-contact ISEs a common source of drift is the formation of a water-layer sandwiched in between the solid-contact transducer (here a carbon-mesh/epoxy composite) and the ISM. Figure 4B shows the normalized results (matching the corresponding start *emf*/mV to 100 mV) of the water-layer test for both PVC-Mg^{2+}-ISE (red trace) and 3Dp-Mg^{2+}-ISEs, respectively. The Mg^{2+}-ISEs were placed in a 1 mM solution of Mg^{2+} for 3 hours before being immersed in a solution of an interferant (K^+) for three hours. Lastly, the Mg^{2+}-ISEs were returned to the 1 mM solution of Mg^{2+}. Here we see that the *emf* observed for the PVC-Mg^{2+}-ISE had similar drift (~1.3 mV/h) prior to switching to the interfering solution, as well as some drift once returned to the Mg^{2+} solution. The *emf* value also did not return to original *emf* recorded prior to immersion in the interfering solution, which is strongly

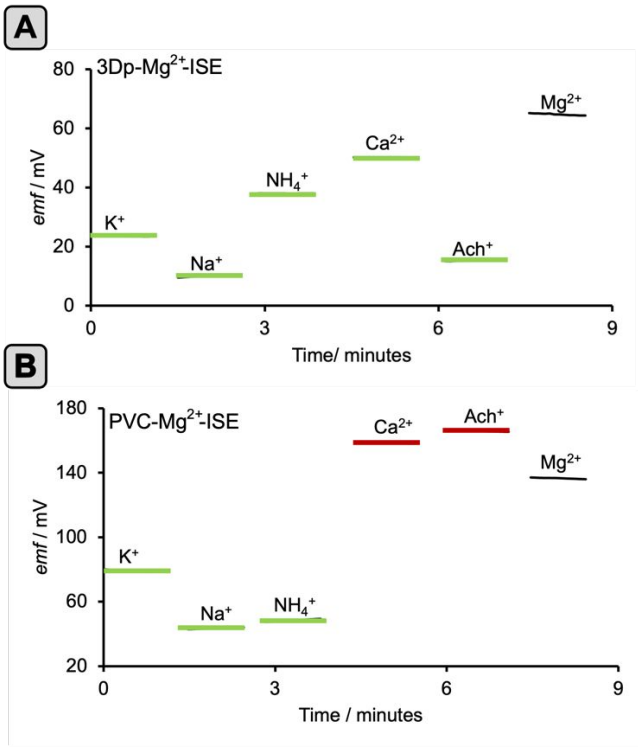

Figure 3. Selectivity analysis showing the *emf* readings obtained for 1.0 mM K^+, Na^+, NH_4^+, Ca^{2+}, Ach^+, and Mg^{2+} versus time. A. *emf* response for 3Dp-Mg^{2+}-ISE. B. *emf* response for PVC-Mg^{2+}-ISE.

Table 3. Selectivity coefficients for biologically relevant interfering cations versus Mg^{2+} for 3Dp-Mg^{2+}-ISE and PVC-Mg^{2+}-ISE.

Interferent	Concentration (M)	Log K 3Dp-Mg^{2+}-ISE	Log K PVC-Mg^{2+}-ISE
Potassium	0.001	-1.38	-1.49
Sodium	0.001	-1.82	-4.27
Ammonium	0.001	-0.89	-3.87
Calcium	0.001	-1.98	1.72
Acetylcholine	0.001	-1.65	5.28
Magnesium	0.001	0	0

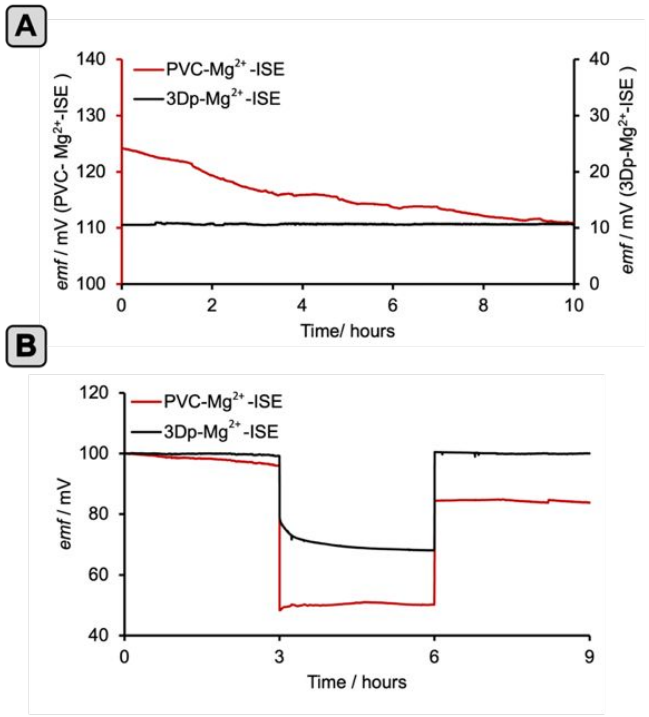

Figure 4. A. The *emf* response of both the PVC-Mg^{2+}-ISE (red trace) and 3Dp-Mg^{2+}-ISE (black trace) in 1 mM Mg^{2+} monitored over a 10 h timespan. B. Normalized results of the water layer test for 3Dp-Mg^{2+} ISE immersed in 1 mM Mg^{2+} for 3 h, then in 1 mM KCl for 3 h then back in 1 mM Mg^{2+} for 3 h.

indicative of the formation of a water-layer. In contrast, the *emf* response of the 3Dp-Mg^{2+}-ISE displayed extreme stability before and after immersion in the interfering solution and the *emf* returned to the pre-interfering solution level. These results suggest that solid-contact ISEs composed of 3Dp-ISMs are highly resilient towards the formation of deleterious water-layers, as has been observed for other ISEs composed of 3Dp-ISMs (24).

3.4 Biofluid Analysis

To validate the reliability and utility of the developed 3Dp-Mg^{2+}-ISEs and investigate any negative impacts related to long-term immersion in biological fluid (i.e., biofouling), a series of calibrations were performed before and after 12-hour exposure of the Mg^{2+}-ISEs to i) sweat, ii) saliva, and iii) urine. Figure 5A shows that the 3Dp-Mg^{2+}-ISEs was most affected by exposure to sweat (red trace), where a shift of approximately 12 mV (versus the control, black trace) was observed across the linear range. Regardless of this shift in *emf*, the 3Dp-Mg^{2+}-ISEs responded in a Nernstian fashion (27.9 mV/decade) and maintained excellent linearity.

Exposure to saliva and urine had a less impactful effect, where the *emf* shifted only 5 and 2 mV, respectively. Here, linearity was maintained although slight decreases in the slope were observed for the 3Dp-Mg^{2+}-ISEs after exposure to saliva (24.7 mV/decade) and urine (26.7 mV/decade). As can be seen in Figure 5B, PVC- Mg^{2+}-ISEs experienced significant shifts in *emf* after immersion in sweat (~63 mV), saliva (~147 mV) and urine (~98 mV). Moreover, significant deviations in both linearity and Nernstian behavior were observed,

where the PVC-Mg^{2+}-ISEs exhibited slopes of 18.9 mV/decade (R^2 = 0.988), 16.6 mV/decade (R^2 = 0.991) and 29.4 mV/decade (R^2 = 0.939) after immersion in sweat, saliva and urine, respectively.

To gain further insights into the potential effect of biofouling on short term analysis (~30 minutes), stability experiments were performed for the 3Dp-Mg^{2+}-ISEs and PVC-Mg^{2+}-ISEs in sweat, saliva and urine, each containing 1 mM Mg^{2+}. Figure 6 shows the normalized (each Mg^{2+}-ISE starts at the same *emf*, denoted 0) responses over a period of 30 minutes for stability experiments performed in sweat (Figure 6A), saliva (Figure 6B) and urine (Figure 6C). Here, we see gradual drifts in the *emf* across each biofluid tested with the PVC-Mg^{2+}-ISEs, being the most pronounced in saliva and sweat. In comparison, 3Dp-Mg^{2+}-ISEs exhibited much more stability throughout the course of the experiment, remaining within < 1 mV. To rationalize these differences in both stability (Figure 6) and reproducibility (Figure 5), contact angle measurements were performed to determine the differences in hydrophobicity between the 3Dp-Mg^{2+}-ISMs and the PVC-Mg^{2+}-ISMs.

Being composed of abundant hydrophobic molecules (e.g., proteins), the phenomena of biofouling has been shown to be promoted on hydrophobic surfaces [52]. Hydrophobicity can be qualitatively determined via water contact angle measurements, where contact angles greater than 90° are representative of a hydrophobic surface [30]. Figure SI.3 shows that the contact angle for the PVC-Mg^{2+}-ISM is ~88°, whereas the contact angle for the 3Dp-Mg^{2+}-ISM is significantly lower at ~59°. These results suggest that the differences in hydrophobicity between the PVC-Mg^{2+}-ISM and the 3Dp-Mg^{2+}-ISM are responsible for the better resilience towards biofouling observed with the 3Dp-Mg^{2+}-ISEs.

4. Conclusions

In this work, we fabricated the first potentiometric sensor for Mg^{2+} using the rapidly emerging technology of 3D printing. The 3Dp-Mg^{2+}-ISE, which consists of a 3Dp-Mg^{2+}-ISM affixed to a 3D printed housing containing a carbon-mesh/epoxy composite, was successfully integrated into a 3D printed microfluidic device. The 3Dp-Mg^{2+}-ISE responded in a Nernstian fashion (slope of 27.5 mV/decade) with a linear range of 1.0 mM – 39 μM and was capable of measuring Mg^{2+} levels covering the physiologically relevant concentrations found in various non-invasively collected biological fluids (i.e., sweat, saliva and urine). Comparisons to PVC-Mg^{2+}-ISEs demonstrated the utility of 3D printing towards ISE fabrication as evidenced by ii) resilience

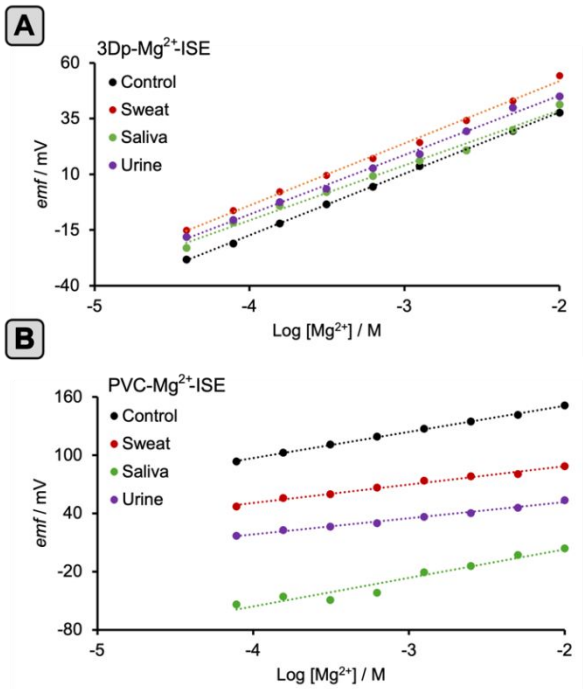

Figure 5. Evaluation of 3Dp-Mg^{2+}-ISEs and PVC-Mg^{2+}-ISEs performance after exposure to biological fluids. A. Calibration curves for 3Dp-Mg^{2+}-ISEs. B. Calibration curves for PVC-Mg^{2+}-ISEs.

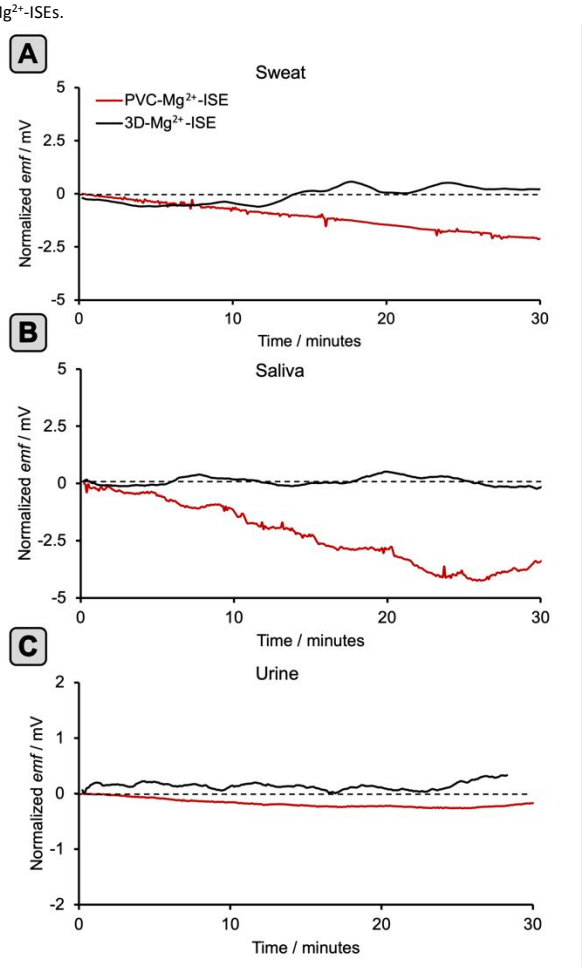

Figure 6. The normalized responses over a period of 30 minutes for stability experiments performed in A. Sweat. B. Saliva. C. Urine.

towards water-layer formation, iii) linear range and iv) improved performance in biological fluids. The ability to rapidly print/test/optimize, afforded by 3D printing, is an extremely useful approach for the fabrication of highly functional potentiometric sensors. Moreover, 3D printing affords a degree of reproducibility in the printing of functional components (i.e., ISMs), which translates to sensor reproducibility. Exploiting 3D printing towards microfluidic device fabrication as well as the fabrication of 3Dp-ISEs can lead to significantly streamlined manufacturing, as well as be conducive towards modifiability and miniaturization. While this work focused on the development and investigation of a 3Dp-Mg^{2+}-ISE integrated into a microfluidic device, in-depth studies related to the differences in selectivity between PVC-Mg^{2+}-ISEs and 3Dp-Mg^{2+}-ISEs, long-term stability and appropriate storage conditions are objectives of our future work.

Author Contributions

CRediT Authorship Contribution Statement: Sarah Farahani: Conceptualization, Formal analysis, Investigation, Writing – original draft, Writing – review & editing. **Dalton L. Glasco:** Formal analysis, Investigation, Writing – review & editing. **Manar M. Elhassan:** Formal analysis, Investigation, Writing – original draft. **Sireesha Pedaballi:** Writing – original draft. **Jeffrey G. Bell:** Conceptualization, Funding acquisition, Methodology, Project administration, Resources, Supervision, Validation, Writing – review & editing.

Conflicts of interest

The authors declare that they have no known competing financial interests or personal relationships that could have appeared to influence the work reported in this paper.

Data Availability

All data and device designs are available in the main text or the ESI.

Acknowledgements

S. Farahani, D. L. Glasco and J. G. Bell acknowledge partial support from the Washington Research Foundation (Ionic Biomarkers Related to Human Healthcare) grant number GR00011963. M. M. Elhassan acknowledges support by the United States Agency for International Development (USAID) grant number G400001016.

Notes and references

1. F. I. Wolf, A. Cittadini, *Mol. Asp. Med.*, 2003, **24**, 3.
2. A. M. Al Alawi, S. W. Majoni, H. Falhammar, *Int J Endocrinol.*, 2018, **10**, 1155.
3. E. D. Ehrenpreis, G. Jarrouj, R. Meader, C. Wagner, M. Ellis, *Disease-a-Month*, 2022, **68**,2.
4. D. Fiorentini, C. Cappadone, G. Farruggia, C. Prata, *Nutrients*, 2021, **13**, 4.
5. W. Cheungpasitporn, C. Thongprayoon, Q. Qian, *Mayo. Clin. Proc.*, 2015, **90**, 8.
6. B. Chernow, *Chest*, 1989, **95**, 6.
7. S. Narayanan, P. Scalici, *Hosp. Pediatr.*, 2015, **5**, 1.
8. F. Ahmed, A. Mohammed, *Med. Sci.*, 2019, **7**, 4.
9. Ryzen, E., Elbaum, N., Singer, F. R., & Rude, R. K, *Magnesium.*, 1985, *4*, 137.
10. Reddy, S. T., Soman, S. S., & Yee, J. *Adv Chronic Kidney Dis.*, 2018,*25*, 224.
11. S. V. Copaja, N. S. Vesna, D. Véliz, *J. Chil. Chem. Soc.*, 2014, **59**, 1, 2366.
12. B. Paull, M. Macka, P. R. Haddad. *J. Chromatogr. A,* 1997, **789**, 329.
13. H. H. Sky-Peck, *Clin. Chem.*, 10, **5**, 391.
14. F. Akhter, A. Nag, M. E. E. Alahi, H. Liu, S. C. Mukhopadhyay, *Sens. Actuator. A Phys.*, 2020, **15**, 305.
15. X. Gao, H. Huang, S. Niu, H. Ye, Z. Lin, B. Qiu, G. Chen, *Anal. Methods*. 2012, **4**, 4.
16. L. Lvova, C. G. Gonçalves, C. Di Natale, A. Legin, D. Kirsanov, R. Paolesse, *Talanta*, 2018, **179**, 430.
17. M. H. Abernethy, R. T. Fowler*, Clin. Chem.,* 1982, **28**, 3, 520.
18. V. Trapani, M. Schweigel-Röntgen, A. Cittadini, F. I. Wolf, *Methods in Enzymol.*, 2012, **505**, 421.
19. M. Liu, X. Yu, M. Li, N. Liao, A. Bi, Y. Jiang, S. Liu, Z. Gong, W. Zeng, *RSC Adv.*, 2018, **8**, 23.
20. I. C. Samper, C. J. McMahon, M. S. Schenkel, et al., *Anal. Chem.*, 2022, **94**, 11.
21. O. Amor-Gutiérrez, E. Costa-Rama, M. T. Fernández-Abedul, *Sensors*, 2022, **22**, 16.
22. A. B. Abdallah, A. Saher, A. F. S. Molouk, W. I. Mortada, M. E. Khalifa, *Biosens. Bioelectron.*, 2022, **208**, 114213.
23. E. Bakker, M. Telting-Diaz, *Anal. Chem.*, 2002, **74**, 12.
24. M. Ghalkhani, N. K. Bakirhan, S. A. Ozkan, *Crit. Rev. Anal. Chem.*, 2020, **50**, 6.
25. D. L. Glasco, N. H. B. Ho, A. M. Mamaril, J. G. Bell, *Anal. Chem.*, 2021, **93**, 48.
26. M. Guzinski, E. Lindner, B. Pendley, E. Chaum, *Anal. Chim. Acta.*, 2021, **1171**, 338642.
27. R. M. Cardoso, C. Kalinke, R. G. Rocha, et al., *Anal. Chim Acta*. 2020, **1118**, 73-91.
28. A. M. Mamaril, D. L. Glasco, F. A. Leal Yepes, J. G. Bell, *ECS Sens. Plus.*, 2022, **1**, 040601.
29. N. H. B. Ho, D. L. Glasco, J. G. Bell, *ECS Sens. Plus.*, 2022, **1**, 020601.
30. M. M. Elhassan, D. L. Glasco, A. Sheelam, A. M. Mahmoud, M. A. Hegazy, S. Mowaka, J. G. Bell, *Biosens. Bioelectron.*, 2024, **248**, 115971.
31. N. H. B. Ho, D. L. Glasco, R. N. Sopp, J. G. Bell, *ECS Trans.*, 2022, 109, **15**, 29.
32. A. Sierra, A. G. Crevillen, A. Escarpa, *Electrophoresis.*, 2019, 40, **1**, 113.
33. Sharma, B., & Sharma, A. *Adv. Eng. Mater.*, 2022, *24*, 2100738.
34. Sajeesh, P., & Sen, A. K. *Microfluid. Nanofluidics.,* 2014, 17, 1.

35. D. Erne, N. Stojanac, D. Ammann, P. Hofsetter, E. Pretsch, W. Simon, *Helv. Chim. Acta*, 1980, **63**, 2271.
36. M. Sejdini, K. Meqa, N. Berisha, E. Citaku, N. Aliu, S. Krasniqi, S. Salihu, *Int. J. Dent*., 2018, **10**, 1155.
37. G. Singh, E. Iyer, H. Malik, *Med. J. Armed Forces India*., 1994, **50**, 4, 261.
38. H. Zhao, X. Zhang, Y. Qin, et al., *Adv. Funct. Mater*., 2023, **33**, 9.
39. T. Kim, Q. Yi, E. Hoang, R. Esfandyarpour, *Adv. Mater. Technol*. 2021, **6**, 4.
40. M. J. Patterson, S. D. R. Galloway, M. A. Nimmo, *Exp. Physiol*., 2000, **85**, 6, 869.
41. R. H. Adrian, et al., *Rev. Physiol. Bioch. P.*, 1977, **79**, 51-131.
42. S. Xu, L. Luo, H. He, H. Liu, L. Cui, *Pol. J. Environ. Stud*., 2015, **24**, 5, 2269-2275.
43. A. A. Al-Jumaili, A. A. Ali, *Iraqi J. Pharm. Sci.*, 2010, **19**, 1, 58.
44. S. H. Kirsch, W. Herrmann, Y. Rabagny, R. Obeid, *J. Chromatogr. B Analyt. Technol. Biomed. Life Sci*., 2010, **878**, 32, 3338.
45. Gupta, V. K., Chandra, S., & Mangla, R. *Sens Actuators B Chem.,* 2002,86, 235.
46. Gupta, V. K., Prasad, R., & Kumar, A. *Talanta*, 2004,*63*, 1027.
47. Saleh, M. B. *J. Electroanal. Chem.*,1994, *373*, 89.
48. Saurina, J., Lopez-Aviles, E., Le Moal, A., & Hernandez-Cassou, S. *Anal. Chim. Acta*.,2002 *464*, 89.
49. Peper, S., Telting-Diaz, M., Almond, P., Albrecht-Schmitt, T., & Bakker, E. *Anal. Chem.,*2002,*74*, 1327.
50. Zamani, H. A., Nezhadali, A., & Saghravanian, M. *Anal. Lett.*, 2008,*41*, 2727.
51. Singh, A. K., Saxena. P., & Panwar. A, *Sens Actuators B Chem.,* 2005,*110*, 377.
52. L. Qi, R. Liang, T. Jiang, W. Qin, *TrAC - Trends Anal. Chem*., 2022, **150**, 116572.

Data Availability Statement

All data and device designs are available in the main text or the ESI.

Manuscript: LC-ART-05-2024-000407.R1

Tribute to George Whitesides

It is an honor to contribute to this special collection of articles celebrating the 85th birthday of George Whitesides. I was fortunate to have spent three years in the Whitesides' group from 2017 to 2020 where my interests in low-cost diagnostics and microfluidic devices were inspired by George.

One thing that specifically sticks out regarding my time in the group was a sense of excitement going into the lab every day. With so many interesting and diverse projects constantly ongoing, there was always this feeling that an important breakthrough was around the corner. Beyond research, George is a gifted mentor who can not only inspire his students but to get them to think about solving problems using unconventional approaches.

I will always look back fondly on my time in the Whitesides' group and consider it a truly transformative time in my scientific career. *Jeffrey G. Bell*.